Earth Surface Processes and Landforms
Earth Surf. Process. Landforms **30**, 1007–1024 (2005)
Published online in Wiley InterScience (www.interscience.wiley.com). **DOI:** 10.1002/esp.1259

Erosion rates driven by channel network incision in the Bolivian Andes

Elizabeth B. Safran,[1]* Paul R. Bierman,[2] Rolf Aalto,[3] Thomas Dunne,[4] Kelin X. Whipple[5] and Marc Caffee[6]

[1] *Environmental Studies Program, Lewis & Clark College, 0615 SW Palatine Hill Road, Portland, OR 97219, USA*
[2] *Department of Geology and School of Natural Resources, University of Vermont, Burlington, VT 05405, USA*
[3] *Department of Earth and Space Sciences, University of Washington, Seattle, WA 98195, USA*
[4] *Donald Bren School of Environmental Science and Management, University of California, Santa Barbara, Santa Barbara, CA 93106, USA*
[5] *Department of Earth, Atmospheric, and Planetary Sciences, Massachusetts Institute of Technology, Cambridge, MA 02139, USA*
[6] *Center for Accelerator Mass Spectrometry, Lawrence Livermore National Laboratory, Livermore, CA 94550, USA. Now at: Department of Earth and Atmospheric Sciences, Purdue University, West Lafayette, IN 47907, USA*

**Correspondence to: E. B. Safran, Environmental Studies Program, Lewis & Clark College, 0615 SW Palatine Hill Road, Portland, OR 97219, USA.*
E-mail: safran@lclark.edu

Received 1 September 2004;
Revised 28 February 2005;
Accepted 17 March 2005

Abstract

The Bolivian Andes flank one of Earth's major topographic features and dominate sediment input into the Amazon Basin. Millennial-scale erosion rates and dominant controls on erosion patterns in this range are poorly known. To define these patterns, we present 48 erosion rate estimates, derived from analysis of *in situ* ^{10}Be in quartz-bearing alluvium collected from the Upper Beni River basin.

Erosion rates, corrected for the non-uniform distribution of quartz in the sample basins, range from 0·04 mm a^{-1} to 1·35 mm a^{-1} and thus integrate over 10^2–10^4 years. Mean and modal values are 0·42 (standard deviation: 0·29) and 0·2–0·4 mm a^{-1} respectively, within the range of long-term average erosion rates in this area derived from apatite fission track thermochronology (0·1–0·6 mm a^{-1}). Hence, our data do not record any significant variation in erosion rate over the last several million years. Mean and modal short-term erosion rates for the Andes are an order of magnitude lower than rates in the Ganges River headwaters in the High Himalaya and an order of magnitude greater than rates typical of the European Alps.

In the Upper Beni River region of the Bolivian Andes, short-term, basin-averaged erosion rates correlate with normalized channel steepness index, a metric of relative channel gradient corrected for drainage area. Neither normalized channel steepness index nor basin-averaged erosion rate shows strong correlation with mean basin hillslope gradient or mean basin local relief because many hillslopes in the Upper Beni River region are at threshold values of slope and local relief. Patterns of normalized channel steepness index appear primarily to reflect tectonic patterns and transient adjustment to those patterns by channel networks. Climate and lithology do not appear to exert first-order controls on patterns of basin-averaged erosion rates in the Bolivian Andes.

Keywords: erosion rates; Bolivia; Andes; cosmogenic radionuclides

Introduction

Mountain landscape evolution reflects the interplay among tectonics, climate, erosion, and long-wavelength crustal responses to mass loading and unloading (e.g. Stephenson and Lambeck, 1985; Beaumont *et al*., 1992). Documenting erosion patterns within mountain ranges is therefore fundamental to understanding the appearance and behaviour of mountain ranges. Elucidation of erosion patterns and their associated morphologic signatures can highlight the role of climate in mountain exhumation (e.g. Reiners *et al*., 2003), identify loci of recent tectonic activity (e.g. Wobus *et al*., 2003), and illuminate geomorphic responses to known tectonic patterns (e.g. Lavé and Avouac, 2000, 2001).

The Andean mountain chain is one of Earth's major topographic features, and the Bolivian Andes encompass the eastern flank of the Andean plateau at its widest point (Figure 1). The Upper Beni River region contains some of the

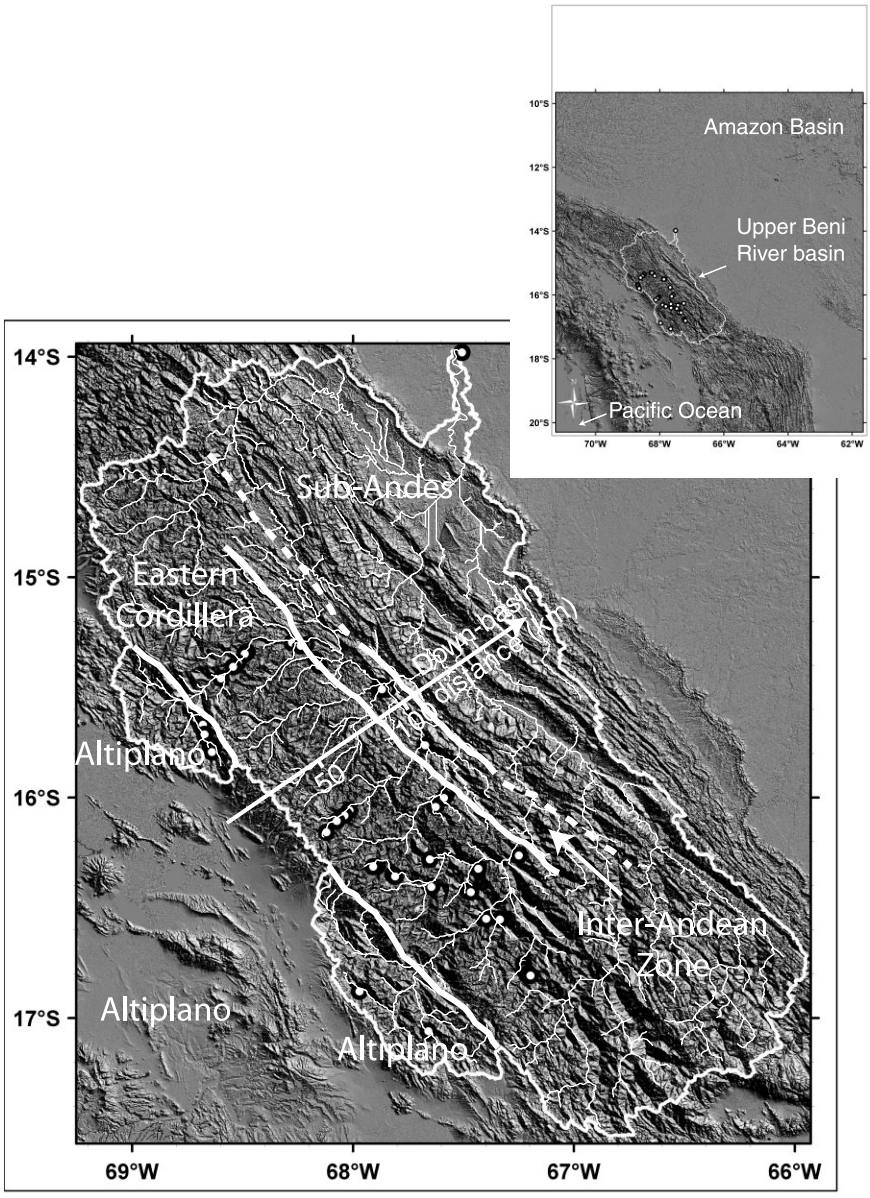

Figure 1. Site map of study area. Maps are shaded relief renderings of a DEM derived from NASA's Shuttle Radar Topographic Mission. Inset map shows location of Upper Beni River basin. Large-scale map shows DEM within a region bounded by the catchment area of the furthest-downstream sample location. Sample sites, major river networks, and boundaries of tectonic provinces are shown.

Bolivian Andes' most dramatic topography and dominates sediment input into the Amazon Basin (Masek *et al*., 1994; Dunne *et al*., 1998; Aalto *et al*., in press). However, the pattern and tempo of erosion that shaped this landscape and the dominant controls on that pattern remain poorly known.

Long-term erosion rates in the region have been derived from apatite and zircon fission track thermochronology (Benjamin *et al*., 1987; Safran, 1998) for only a few locations near the mountain crest where lithologies appropriate for such analyses occur. Moreover, such long-term average erosion rates are not necessarily relevant to morphologic variations in rapidly evolving modern landscapes (e.g. patterns of hillslope or channel gradient; Gabet *et al*., 2003). On the other hand, short-term erosion rates based on sediment yield (Guyot, 1993; Aalto *et al*., in press) or landslide frequency analyses (Blodgett, 1998) are subject to decadal-scale fluctuations and the effects of transient sediment

storage (Trimble, 1977) and may not represent the erosion patterns that shaped the modern landscape (Kirchner *et al*., 2001).

Cosmogenic radionuclides (CRNs), measured in river sediment, have been used to determine spatially integrated erosion rates over timescales of 10^2 to 10^5 years (e.g. Granger *et al*., 1996; Bierman *et al*., 2001; Schaller *et al*., 2001; Matmon *et al*., 2003; Vance *et al*., 2003). Assuming that sediment delivered to channels becomes rapidly mixed and that long-term valley storage is minimal, measurements of ^{10}Be concentration in alluvium can yield average erosion rates for each upstream basin sampled (Brown *et al*., 1995a; Bierman and Steig, 1996; Granger *et al*., 1996). We present 48 erosion rates, derived from analysis of *in situ* ^{10}Be in quartz-bearing alluvium collected from the Upper Beni River basin. Our aims are to determine rates of erosion averaged over thousands of years at a wide range of spatial scales, to identify spatial patterns among these erosion rates, and to identify controls on erosion patterns.

Study Area

The study area lies within the Upper Beni River basin, one of the major trans-range drainages on the eastern flank of the Bolivian Andes (Figure 1). The Bolivian Andes have been divided into four tectono-structural zones (e.g. McQuarrie, 2002): (1) the Altiplano, an internally drained, largely sediment-covered, low-relief plateau with an average elevation of about 3·7 km; (2) the Eastern Cordillera (EC), a bi-vergent, thin-skinned fold and thrust belt that deforms mostly lower Palaeozoic rocks; (3) the Inter-Andean zone (IAZ), similar in structural style to the EC but involving younger rocks and deformation at higher structural levels; and (4) the Sub-Andes (SA), a zone with *c*. 1 km of local relief and significant modern deformation characterized by tight anticlines and broad, sediment-filled synclines. The boundaries of these zones have been defined in two locations: near Cochabamba, just to the SE of the study area, and in the Pilcomayo River Basin in southern Bolivia (McQuarrie, 2002). The approximate locations of tectonic province boundaries in the study area (Figure 1) are based on extrapolation from the Cochabamba cross-section and on Figure 1 of McQuarrie (2002).

To simplify interpretation of CRN concentrations, sample locations were concentrated predominantly within the IAZ and EC, where sediment storage reservoirs are small and turn over rapidly relative to the time period over which the CRNs integrate. The Upper Beni River system also extends into the Altiplano in the headwaters of the Consata and La Paz Rivers. Although these areas now drain eastwards, they are considered as fragments of the Altiplano province in this paper.

The study region is underlain predominantly by fine-grained Ordovician, Devonian, and Silurian sedimentary rocks intercalated with sandy beds (Martinez and Tomasi, 1978; Martinez, 1980). These packages are metamorphosed to varying degrees, locally producing shales, slates, phyllites, schists, sandstones, metagreywackes, and quartzites (Figure 2). Metamorphic grade of schists ranges from biotite to staurolite, andalusite and sillimanite grade. Localized zones of contact metamorphism are associated with several of the Mesozoic and Cenozoic plutons at the NE edge of the plateau, which underlie the highest peaks in the basin (Martinez, 1980). The rocks contain varying amounts and grain sizes of quartz, the mineral we used for ^{10}Be analysis.

Channels throughout most of the Upper Beni River system are steep and generally confined in narrow valley bottoms. Trunk stream gradients near the basin mouth are approximately 0·001, while the maximum gradient of low-order tributaries, with drainage areas of *c*. 1–2 km^2, is *c*. 0·65 (Safran, 1998). Bedrock is commonly exposed on channel banks and beds, and alluvial cover in most places is patchy and thin. Such field evidence indicates that the behaviour and morphology of the channel network is for the most part controlled by the rate of incision into bedrock. The most widespread hillslope geomorphic processes are rapid shallow failures in colluvium or weathered bedrock and slow, deep-seated landsliding in bedrock. Hillslopes are generally steep (*c*. 20–60°) and colluvium is up to 1 m thick.

The climate within the study region ranges from humid to semi-arid. Mean annual rainfall is about 1500–2000 mm in the Sub-Andes. Mean annual rainfall drops to about 500–800 mm near the Altiplano/Eastern Cordillera divide, with the SE and NW portions of the basin headwaters representing the lower and higher end of this range, respectively (Hoffman, 1979).

Sample Collection and Processing

Samples for ^{10}Be analysis were collected from alluvium in active transport. Drainage areas upstream of alluvial sample locations ranged from 1 km^2 to 70 000 km^2, with the majority of basins (*c*. 60 per cent) under 200 km^2 (Table I). Sample locations were chosen to achieve extensive spatial coverage, to sample areas dominated by particular

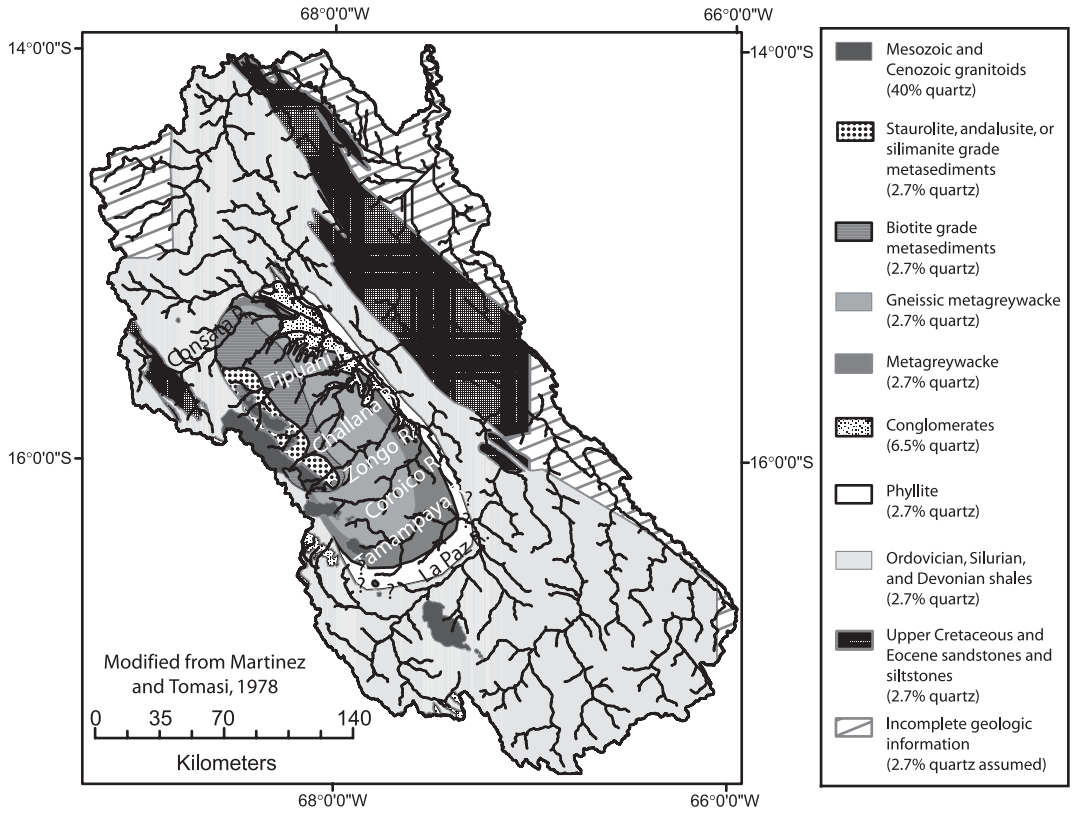

Figure 2. Geological map of the study area, modified from Martinez and Tomasi (1978). Spatial extents of high-grade and biotite-grade metamorphic rocks are from Martinez and Tomasi (1978), while approximate boundaries of low-grade metamorphic facies are based on field observations. Quartz content, determined from published studies and from acid etching experiments (see text), listed in key. A pluton described as containing 70 per cent quartz (Avila-Salinas, 1990) is too small to be seen on the map at this scale and is excluded from the legend.

Table I. Sample locations (datum WGS84), cosmogenic radionuclide (CRN) concentrations and erosion rates, Upper Beni River region

Sample ID*	Longitude	Latitude	Area (km^2)	CRN concentration† (atoms/g)	$^{26}Al/^{10}Be$ ratio	Erosion rate ($mm\ a^{-1}$)
BOL-01	68°38′21·516″ W	15°47′34·296″ S	134	35300 ± 2100		1·34
				[196400 ± 150800]	5·56 ± 4·28	
BOL-02	68°38′10·824″ W	15°46′58·188″ S	42·0	78300 ± 6200		0·45
BOL-03	68°38′47·112″ W	15°45′51·084″ S	16·3	38600 ± 3700		0·66
BOL-04	68°38′45·096″ W	15°45′46·548″ S	<1	36100 ± 3500		0·38
BOL-05	68°40′19·776″ W	15°42′47·448″ S	31·2	30700 ± 2400		0·77
BOL-06	68°40′43·752″ W	15°40′11·712″ S	30·0	132000 ± 8100		0·23
BOL-07	68°30′30·034″ W	15°22′53·652″ S	2930	89100 ± 3000		0·28
				[466600 ± 31500]	5·24 ± 0·39	
BOL-08	68°35′53·160″ W	15°27′30·888″ S	198	90800 ± 3000		0·24
BOL-09	68°32′37·932″ W	15°24′36·036″ S	26·5	38100 ± 3100		0·34
BOL-10	68°29′23·892″ W	15°20′53·916″ S	1·1	93600 ± 5300		0·08
BOL-11	68°28′50·628″ W	15°20′34·044″ S	4·1	24300 ± 3000		0·33
BOL-13	68°16′29·928″ W	15°17′57·228″ S	3230	89200 ± 3300		0·26
				[478300 ± 44600]	5·36 ± 0·54	

(*continued overleaf*)

Table I. (*Continued*)

Sample ID*	Longitude	Latitude	Area (km^2)	CRN concentration† (atoms/g)	$^{26}Al/^{10}Be$ ratio	Erosion rate ($mm\ a^{-1}$)
BOL-14	68°14′14·964″ W	15°18′41·004″ S	432	58600 ± 7800		0·18
BOL-15	68°12′48·348″ W	15°18′29·592″ S	5830	75500 ± 3200		0·27
BOL-16	68°10′0·120″ W	15°22′36·408″ S	120	103000 ± 7900		0·06
BOL-17	68°9′14·112″ W	15°24′5·580″ S	248	38200 ± 2600		0·16
BOL-18	67°52′52·896″ W	15°29′41·136″ S	10900	89000 ± 3400		0·15
BOL-19	67°53′9·348″ W	15°30′8·856″ S	1540	58600 ± 3200		0·53
				[290200 ± 37600]	4·95 ± 0·70	
BOL-20	67°52′4·908″ W	15°30′33·516″ S	1760	33100 ± 2300		0·93
BOL-21	67°50′31·560″ W	15°30′30·420″ S	5360	55900 ± 3700		0·31
BOL-22	67°40′28·992″ W	15°45′46·008″ S	1460	36500 ± 3000		0·60
BOL-23	68°34′37·128″ W	15°58′53·328″ S	25·7	154000 ± 5000		0·04
BOL-24	68°35′19·464″ W	16°0′2·520″ S	154	32300 ± 2600		0·25
				[125200 ± 21400]	3·88 ± 0·73	
BOL-25	67°37′34·424″ W	16°2′36·672″ S	146	53300 ± 3400		0·16
				[271100 ± 42300]	5·09 ± 0·86	
BOL-26	67°39′6·948″ W	16°16′53·184″ S	39·7	44700 ± 2600		0·24
BOL-27	68°7′11·928″ W	16°9′25·344″ S	146	68100 ± 3100		0·56
				[352800 ± 38600]	5·18 ± 0·61	
BOL-28	68°4′27·228″ W	16°6′25·416″ S	127	48100 ± 2400		0·52
BOL-29	68°2′21·120″ W	16°4′57·684″ S	31·9	45700 ± 3300		0·55
BOL-30	68°0′57·024″ W	16°3′27·036″ S	425	66600 ± 3300		0·41
BOL-31	67°58′11·784″ W	16°52′47·316″ S	111	120000 ± 5700		0·23
BOL-32	67°39′33·120″ W	16°3′40·536″ S	834	134000 ± 4300		0·21
				[467000 ± 45600]	3·48 ± 0·36	
BOL-33	67°11′50·964″ W	16°48′28·656″ S	43·7	69900 ± 4700		0·20
BOL-34	67°12′46·332″ W	16°48′4·176″ S	177	57100 ± 5000		0·47‡
BOL-34				40700 ± 3000		
BOL-34				59600 ± 3500		
BOL-35a	67°13′17·508″ W	16°46′44·976″ S	3·4	93400 ± 3400		0·16§
BOL-35b				102500 ± 4800		
BOL-35b				89700 ± 4000		
BOL-35b				88300 ± 3800		
BOL-36a	67°13′49·908″ W	16°45′13·428″ S	21·4	77400 ± 4600		0·20
BOL-36b				75800 ± 3300		
BOL-37	67°20′11·282″ W	16°33′13·824″ S	841	52400 ± 2700		0·62
BOL-38a	67°23′44·484″ W	16°33′0·468″ S	5410	52800 ± 2600		0·50
BOL-38b				54900 ± 2200		
BOL-39	67°28′5·556″ W	16°25′42·852″ S	68·9	81200 ± 3800		0·12
BOL-40	67°28′40·440″ W	16°24′13·320″ S	152	48400 ± 3200		0·28
BOL-41	67°25′59·232″ W	16°19′22·728″ S	1460	18900 ± 1500		1·35
BOL-42	67°14′58·704″ W	16°15′43·848″ S	10400	46900 ± 3000		0·55
BOL-43	67°25′57·000″ W	16°19′13·116″ S	416	41700 ± 2500		0·25
BOL-44	67°38′44·268″ W	16°24′18·648″ S	601	46700 ± 2800		0·64
BOL-45	67°38′32·280″ W	16°24′6·552″ S	348	30500 ± 2400		0·84
BOL-46	67°48′33·012″ W	16°21′26·028″ S	22·8	64200 ± 5500		0·33
BOL-46				67000 ± 4100		
BOL-46				106100 ± 5100		
BOL-48	67°54′31·932″ W	16°18′50·688″ S	62·7	51800 ± 2300		0·62
BOL-49	67°53′31·200″ W	16°18′45·900″ S	59·6	85700 ± 3400		0·41
BOL-50	67°30′22·644″ W	13°58′48·720″ S	70200·0	21500 ± 1200		0·86
				[122300 ± 13900]	5·70 ± 0·72	

* Bold indicates 1–4 mm size fraction; italic indicates >4 mm size fraction. Letters a and b indicate replicate samples.

† Values in square brackets are ^{26}Al concentrations; all others are ^{10}Be concentrations.

‡ Erosion rates for samples with multiple grain size analyses are based on 0·25–1 mm size fraction.

§ Erosion rate for samples with replicates determined using mean ^{10}Be concentration.

hillslope geomorphic processes, and to explore mixing patterns among some nested basins. Lithologies of both alluvial clasts and *in situ* bedrock were noted at each sample site. A quantitative index of unconfined, compressive rock strength was determined for the dominant lithologies exposed at the majority of sample sites using an N-type Schmidt hammer applied to *in situ* bedrock and in-channel boulders.

Quartz was extracted from the 0·25–1 mm grain size fraction of the alluvium for all samples using sequential HF leaching followed by mineral separation and additional leaching (Kohl and Nishiizumi, 1992). For three samples, we also analysed ^{10}Be concentration in the 0·25–1 mm, 1–4 mm, and >4 mm size fractions. No systematic bias in ^{10}Be concentration with grain size was observed (Table I). Replicate analyses were performed for three samples, and the average difference between the ^{10}Be concentrations of the two samples in each pair was 5 per cent (Table I), consistent with the AMS counting statistics for these low-activity samples.

Quartz yields varied widely and for many samples were very low, as little as several per cent. To help us estimate the percentage of quartz in each sample as a proxy for the exposure area of quartz-bearing rocks in each basin, we performed HF/HNO_3 etching experiments to estimate quartz yield. These experiments included 16 samples, with 10 derived from basins underlain only by metasedimentary rocks and six derived from basins draining both plutons and metasedimentary rocks.

We extracted both Be and Al from the quartz using standard methods (Bierman and Caffee, 2002). For all but eight samples, we analysed only ^{10}Be because the concentration of native Al and other cations in most quartz separates, even after extended acid etching and density separation, was very high, typically hundreds of ppm. All analyses were conducted at Lawrence Livermore National Laboratory. Ratios of ^{26}Al/^{10}Be in the eight samples for which we have Al data are lower than the production ratio of 6·0 (Nishiizumi *et al.*, 1989). The ratios range from 3·5 to 5·6 and average $4{\cdot}9 \pm 0{\cdot}8$ (1σ) (Table I). Given the rapid rate at which sediment is generated and the lack of substantial sediment storage in the study area, we interpret these ratios as reflecting incomplete recovery of stable Al (Bierman and Caffee, 2002), rather than burial.

We processed samples in batches of eight. Because we anticipated that blank corrections would be substantial, each batch contained two process blanks containing the same amount of carrier as the samples (250 μg Be). The average ^{10}Be/^{9}Be of these two blanks was subtracted from the measured ratio of the samples in the batch with which the blanks were run. Blanks run over the course of the study averaged $2{\cdot}1 \pm 0{\cdot}7 \times 10^{-15}$ (1σ) ^{10}Be/^{9}Be. The average difference between the two blanks in each batch was 7 per cent ($n = 11$ batches).

Determining Basin-averaged Erosion Rates from ^{10}Be Concentrations

Beryllium-10 concentration among our samples ranges from 19 000 to 154 000 atoms/g (Table I), with a mean value of 63 000 atoms/g and a modal value of 30 000–50 000 atoms/g. The range of measured isotope concentrations drops from 130 000 atoms/g among small (<200 km^2) basins to *c*. 40 000 atoms/g for basins larger than *c*. 2000 km^2, which integrate over the full range of tectonic zones represented in the study area.

To infer erosion rates from raw ^{10}Be concentrations in quartz separated from alluvium, basin-averaged production rates must be known. We determined these by representing each basin as a raster surface. We used neutron-only data to determine production rate in each pixel due to its latitude and elevation (Lal, 1991). We multiplied this production rate by the quartz fraction of the underlying lithology (see below). We summed the resulting values for all pixels in each basin and divided by the sum of the quartz fractions of all pixels in the basin. Finally, we used a quantitative model described in previous studies (e.g. Brown *et al.*, 1995a; Bierman and Steig, 1996; Granger *et al.*, 1996) to derive erosion rates from basin-averaged production rates and measured ^{10}Be concentrations.

Geographical coordinates and elevation were extracted from a digital elevation model (DEM) of *c*. 90 m resolution derived from NASA Shuttle Radar Topographic Mission data. Quartz fraction of each pixel was determined by using a digitized geological map (Martinez and Tomasi, 1978) to identify the underlying rock type and by determining a characteristic quartz fraction for each rock type. Based on petrological work by Avila-Salinas (1990), the quartz content of all plutons, with one exception, was assumed to be 40 per cent. A single small pluton was assigned a quartz fraction of 70 per cent (Avila-Salinas, 1990). All metasedimentary rock was represented with a quartz fraction of 2·7 per cent, the mean value for granitoid-free samples used in our etching experiments (range: <0·5 to *c*. 6 per cent). A late Miocene deposit near the boundary between the IAZ and the Sub-Andes (Figure 2) was represented with a quartz fraction of 6·5 per cent. This value was obtained by determining the approximate drainage area associated with the deposit, determining the fraction of that area underlain by plutons versus metasedimentary rock in the modern landscape, and weighting the relative contributions of each fractional area by the associated quartz fraction. Although the areal extent of exposed plutons may have changed over time, sedimentological evidence suggests these plutons were indeed exposed when the deposit formed (Fornari *et al.*, 1987; Herail and Viscarra, 1988). In any case, the quartz

fraction assigned to this deposit has little effect on inferred erosion rates, as only four sample basins have >10 per cent of their drainage areas underlain by this lithology. We assigned the same quartz fraction to very small areas of conglomerate that crop out in the Altiplano fragments of our study area. Since most of the sediment in both conglomeratic deposits is relatively old (>several Ma), CRN inheritance is unlikely to pose a problem. We lack information about the quartz content of a fifth rock type exposed in the study region, labelled Cretaceous and Tertiary sandstones and siltstones on Figure 2 (Martinez and Tomasi, 1978). We assumed, based on limited descriptions in the literature (Martinez, 1980), that these rocks have approximately the same quartz fraction as the Palaeozoic metasedimentary rocks. Only four sample basins have >10 per cent of their drainage areas underlain by this lithology, and the erosion rate estimates derived from them lie within the modal range of values for the whole dataset (see below). In portions of the study area for which geological information is incomplete (Figure 2), a 2·7 per cent quartz content was assumed. This assumption affects only the erosion rate estimate for the single largest basin sampled.

We did not include muons in the calculation of production rates. Because the basins we sampled are at high elevation and muon-induced surface production rates are only several per cent of neutron rates even at sea level (Brown *et al*., 1995b), disregarding muons should result in errors much less than those associated with measurements and assumptions inherent in the interpretation of cosmogenic data from fluvial samples. Furthermore, because of the current uncertainty in the elevation–depth production function for muons, any muon calculations would themselves have carried significant uncertainty (Granger and Smith, 2000; Heisinger *et al*., 2002a,b).

Erosion Rates in the Upper Beni River Region

Using values of 2·7 g cm^{-3} for substrate density and 165 g cm^{-2} for the characteristic attenuation rate for fast neutrons, we obtained erosion rates ranging from 0·04 mm a^{-1} to 1·35 mm a^{-1}, with a mean and standard deviation of 0·43 and 0·29 mm a^{-1}, and a mode of 0·2–0·4 mm a^{-1} (Figure 3). Correcting for local quartz fraction made a relatively small difference to the overall frequency distribution of erosion rates, although a few erosion rates changed by up to *c*. 70–80 per cent (Figure 3c). In all but two of the basins showing a >20 per cent difference between corrected and uncorrected erosion rate estimates, quartz-rich lithologies occupy high terrain, and the correction resulted in an increase in the estimated erosion rate.

The central tendency of our data resembles that of long-term average erosion rates derived from apatite fission track (AFT) thermochronology on samples from three valleys in the same area. AFT-based erosion rates average over 5–20 Ma and range from *c*. 0·1 to 0·6 mm a^{-1}, with a mean of 0·3 mm a^{-1} and a mode of 0·1–0·2 mm a^{-1} (Benjamin *et al*., 1987; Safran, 1998). On average, therefore, our CRN data do not imply substantial variation in erosion rate over the last several million years in the Upper Beni River region. Our sampling scheme does not permit direct comparison of long- and short-term average erosion rates for most individual localities, but in the headwaters of the Zongo River valley, modern rates of 0·40–0·55 mm a^{-1} exceed long-term average rates by about 15–100 per cent (Figure 4). The CRN-derived erosion rate for the Taquesi River basin is 8 per cent lower than, to 100 per cent higher than, long-term rates of 0·30–0·65 mm a^{-1} derived from AFT analysis of rocks in the headwaters of the basin (Figure 4). Long-term erosion rates are lowest in the Challana River basin (0·15–0·35 mm a^{-1}), where the CRN-derived erosion rate is highest (0·95 mm a^{-1}), but the discrepancy between locations of the two sample types in this basin is so great that no conclusions can be drawn about temporal variations in erosion rate. Overall, our data suggest that the relative magnitude of long-term and short-term rates implied by models of tectonic or climatic change in the Bolivian Andes should be consistent with at most a modest increase in erosion rate towards the present.

Mean and modal erosion rates from the Upper Beni River region are nearly an order of magnitude lower than CRN-derived erosion rates in the headwaters of the Ganges River in the High Himalayas (*c*. 3 mm a^{-1}; Vance *et al*., 2003). Maximum erosion rates in our study area are comparable to those found in the Himalayan foothills and on the edge of the Tibetan plateau (0·8–1·2 mm a^{-1}; Vance *et al*., 2003). Mean and modal values in our study area are comparable to the highest CRN-based erosion rates measured in the European Alps (*c*. 0·1 mm a^{-1}) but are an order of magnitude greater than typical Alpine erosion rates (*c*. 0·02–0·04 mm a^{-1}; Schaller *et al*., 2001).

Links Between Erosion Rate and Landscape Morphology

Over the long term, rates of mountain erosion are controlled by rates of channel incision into bedrock (e.g. Seidl and Dietrich, 1992; Howard *et al*., 1994; Whipple, 2004). Channel incision rates are a function of discharge and local channel gradient (e.g. Howard and Kerby, 1983), and channel gradient reflects lithology and rock uplift rate. All else being equal, patterns of channel gradient are indicators of relative channel incision rates. One useful metric of relative

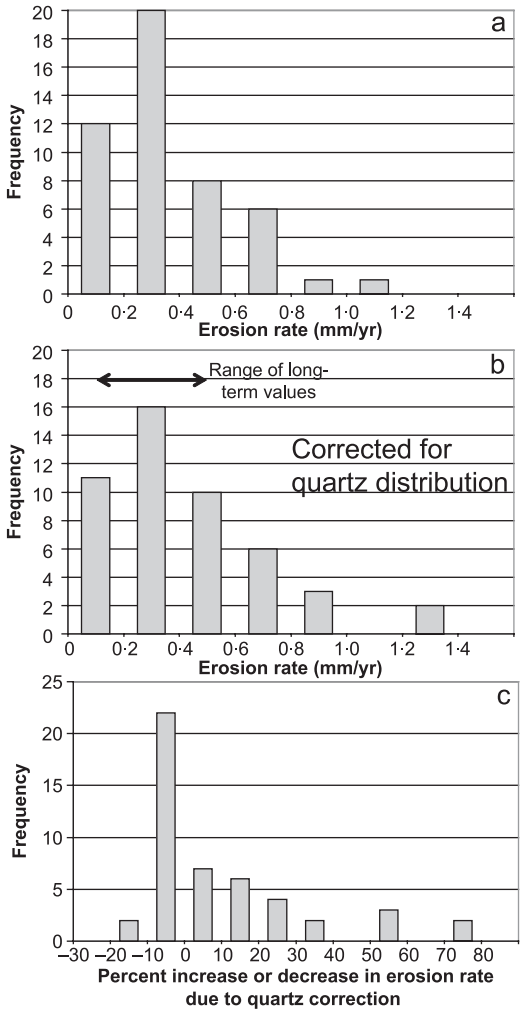

Figure 3. Frequency distribution of erosion rates estimated from ^{10}Be concentrations, and significance of the quartz correction. (a) Frequency distribution of erosion rates assuming a uniform distribution of quartz throughout the study region. (b) Frequency distribution of erosion rates corrected for quartz fraction of underlying lithology. (c) Frequency distribution of percentage differences between uncorrected and corrected erosion rates.

gradient is channel steepness index, k_s, the coefficient modifying a power law relationship between local channel gradient (S) and contributing drainage area (A) (e.g. Flint, 1974):

$$S = k_s A^{-\theta} \tag{1}$$

where θ is the concavity index. Channel steepness index is preferable to θ as a metric of channel morphology because it has been shown to be sensitive to variations in rates of rock uplift (Snyder *et al.*, 2000; Kirby and Whipple, 2001; Kirby *et al.*, 2003; Wobus *et al.*, in press). It has thus been used to define, qualitatively, zones characterized by differences in rates of tectonically driven channel incision (e.g. Kirby *et al.*, 2003; Wobus *et al.*, 2003).

To determine whether CRN-derived erosion patterns reflect channel incision patterns, we determined representative k_{sn} values – k_s normalized to a reference concavity index of 0·45 (necessary for inter-comparison; see Sklar and Dietrich, 1998; Wobus *et al.*, in press) – for as many basins as possible (75 per cent), and plotted erosion rate against k_{sn} (Figure 5). Values of k_{sn} were defined by performing power-law regressions on distinctive segments of S and A plots (as described by Wobus *et al.*, in press). We excluded basins for which a single k_{sn} value was clearly inappropriate and basins with drainage areas <3 km^2, since basins smaller than that do not exhibit characteristically fluvial

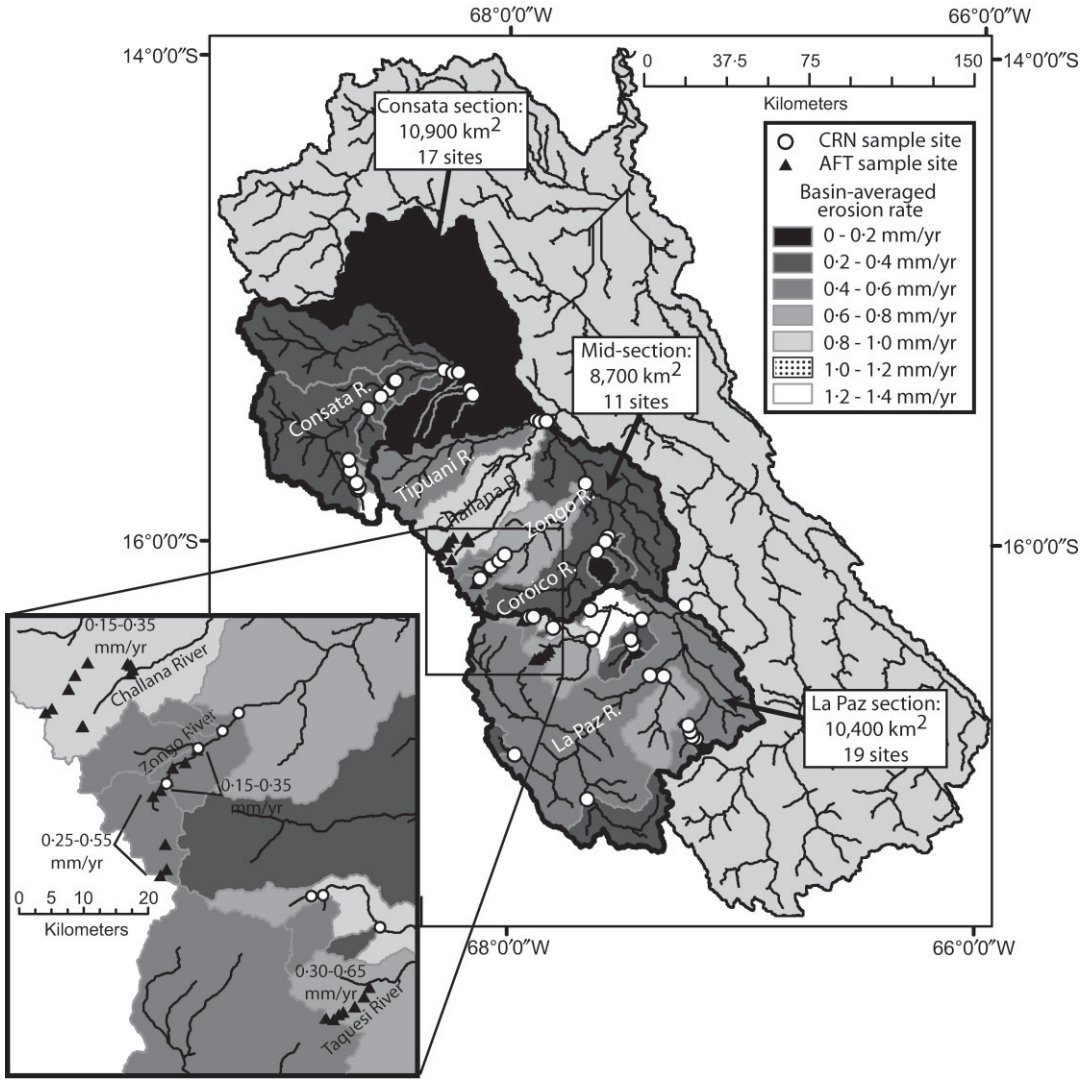

Figure 4. Map view of basin-averaged erosion rate corrected for quartz content. Locations of along-strike (or cross-basin) sections for which erosion rate patterns were examined are shown in heavy black outline. These outlines represent drainage divides of: (1) Consata River system; (2) combined Tipuani, Challana, Zongo and Coroico River systems; and (3) a portion of the La Paz River system. Shading represents CRN-based, basin-averaged erosion rates. Inset shows sample sites and results of AFT analysis.

slope–area scaling (e.g. Tarboton *et al*., 1989; Montgomery and Foufoula-Georgiou, 1993; Stock and Dietrich, 2003). We also excluded two basins for which erosion rate estimates appeared to be anomalous because they were not consistent with those from nested basins.

There is a correlation between erosion rate and k_{sn} for the entire data set (Figure 5; $p = 0{\cdot}05$). Because apatite fission track data suggest that long-term erosion rate varies by several tenths of a millimetre per year along-strike (i.e. across basin) in the Upper Beni River region (Safran, 1998), we explored whether along-strike differences in modern erosion rate pattern occur. We divided our sample basins into three cross-basin sections. The sections are centred on the Consata River system, the La Paz River system, and a mid-section that includes the Tipuani, Challana, Zongo and Coroico River systems (Figure 4). Erosion rate as a function of normalized channel steepness index within each section is represented in Figure 5.

Although there is considerable scatter in the relationship between erosion rate and normalized channel steepness index, the linear models fitting each along-strike section are similar, and there is no obvious deviation from the overall

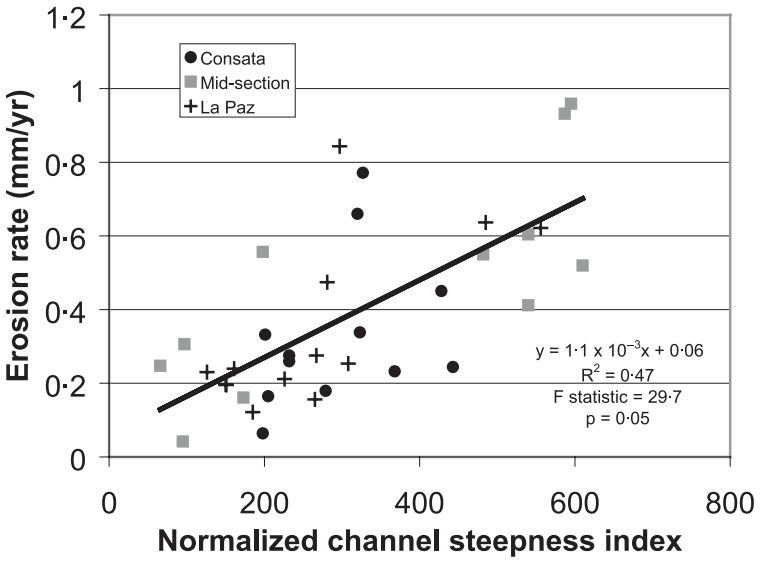

Figure 5. Basin-averaged erosion rate as a function of normalized channel steepness index. Correlation shown is for overall dataset. Symbol shade and shape corresponds to along-strike sections shown in Figure 4.

trend in any section (Figure 5). This suggests that k_{sn} is a good metric for channel incision rate, and that patterns of channel incision exert an important influence on basin-averaged erosion rate throughout the study area.

Normalized channel steepness index ranges from 40–200 in the uppermost several kilometres of streams in the Upper Beni River region to >300 some 10–20 km downstream to 40–200 in the lowermost portion of the EC and in the IAZ (Figure 6). In the La Paz and Consata Rivers, maximum normalized channel steepness index values are 300–400, compared to 400–600 in the rivers of the mid-section, and maxima are shifted upstream relative to those in the mid-section.

The correlation between k_{sn} and erosion rate combined with the spatial pattern of k_{sn} in the study area implies that, to first order, erosion rate should decrease down the axis of the basin. A plot of erosion rate against down-basin distance of the basin midpoint for a subset of sample basins reveals a statistically significant ($p = 0{\cdot}05$) decrease in erosion rate with down-basin distance (Figure 7a). Basin midpoint is defined as the point on the sample basin's channel network at which upstream drainage area is closest to half the total basin area. Down-basin distance is defined along an axis with an arbitrary origin that runs parallel to the trunk streams of the Upper Beni River region (Figure 1). Since down-basin position is not well described by a single point for large basins, basins with drainage areas >1000 km^2 were excluded from the plot.

Erosion rates range from 0·2 to 1·35 mm a^{-1} near the crest of the range, to 0·05 to 0·25 mm a^{-1} at down-basin distances of 70–100 km. Although the most quartz-rich lithologies occur near the crest of the range, there is no systematic relationship between basin-averaged erosion rate and fraction of basin area underlain by these lithologies. Hence, Figure 7 seems to reflect patterns in landscape processes rather than incomplete correction for the distribution of quartz in the sample basins. Spatial patterns of k_{sn} indicate that down-basin erosion patterns should vary among sections (Figure 6), and Figure 7b confirms this expectation.

In contrast to the correlation between erosion rate and normalized channel steepness index, measures of hillslope morphology do not correlate strongly with basin-averaged erosion rate. There is no relationship between erosion rate and mean basin slope (Figure 8a) and only a weak correlation between basin-averaged erosion rate and mean basin local relief (Figure 8b). Slope for each pixel is calculated within a 150 m × 150 m neighbourhood (using a DEM resampled to 50 m pixel size), and local relief for each pixel is calculated by subtracting the highest and lowest elevations within a circular neighbourhood 5 km in diameter. The lack of correlation between basin-averaged erosion rate and hillslope morphology has multiple possible causes. In places where channel incision is rapid, hillslopes may be at threshold values of gradient and local relief (e.g. Strahler, 1950; Schmidt and Montgomery, 1995; Burbank *et al.*, 1996; Roering *et al.*, 2001; Montgomery and Brandon, 2002). Under such conditions, channel incision rate is reflected in the frequency of landsliding rather than in adjustments to hillslope morphology (e.g. Strahler, 1950; Schmidt and Montgomery, 1995; Burbank *et al.*, 1996; Roering *et al.*, 2001; Montgomery and Brandon, 2002). Alternatively, there may be locations where the local landscape is in a transient state of response to an external forcing mechanism (e.g.

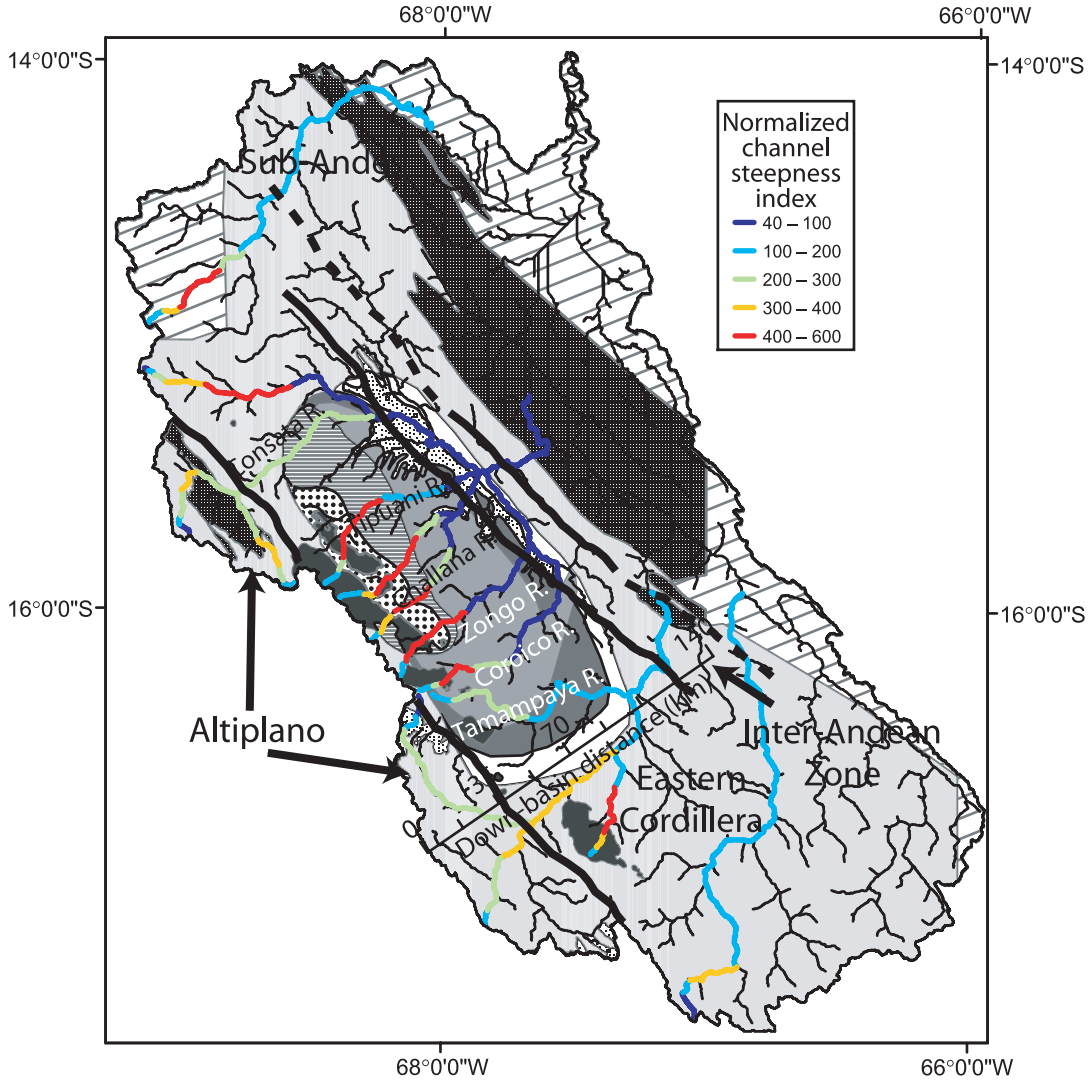

Figure 6. Spatial patterns of normalized channel steepness index, displayed for select streams in the Upper Beni River region. Streams are colour-coded by normalized channel steepness index. Legend for geological base map is the same as for Figure 2.

change in uplift rate, or regional climatic change), and hillslope morphology has not yet adjusted to local channel incision rates.

Plots of mean basin local relief and mean basin slope against normalized channel steepness index suggest hillslope morphology in the Upper Beni River region reflects both gradient and local relief thresholds and transient adjustment to local channel incision rates (Figure 9). For normalized channel steepness indices of >300, mean basin slope and mean basin local relief reach maxima at 55 per cent (*c*. 29°) and 1500 m, respectively, suggesting hillslopes are at landsliding threshold conditions. Field observations confirm that landsliding is widespread in areas of k_{sn} greater than *c*. 200. Local relief appears to dip below the maximum regional value in areas where $k_{sn} > 500$ (Figure 9b), suggesting that local relief in some basins may not yet have responded to a relatively recent increase in local channel incision rate.

In summary, basin-averaged erosion rate correlates with normalized channel steepness index. The spatial pattern of k_{sn} results in a general down-basin decrease in erosion rate. Erosion rate is not clearly reflected by hillslope morphology. The weakness of the correlation between basin-averaged erosion rate and hillslope morphology likely reflects threshold values of hillslope gradient and local relief as well as local transience in hillslope response to channel incision.

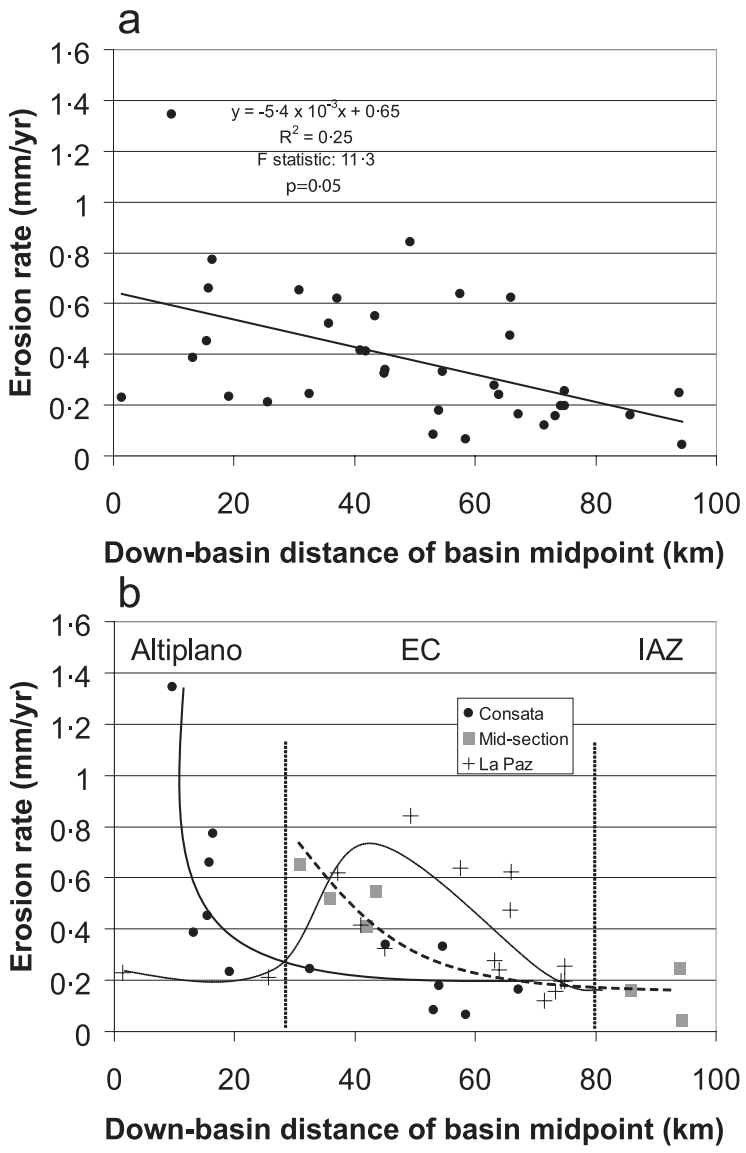

Figure 7. Erosion rate as a function of down-basin distance. Points are plotted at the down-basin location of the basin midpoint, defined in the text. Basins larger than 1000 km^2 are excluded from both plots. (a) Linear fit to data from all sections. (b) Cross-basin sections indicated by symbol shade and shape. Approximate down-basin locations of tectonic province boundaries defined by McQuarrie (2002) are shown as vertical lines. Solid, dashed and dotted curves indicate trends through Consata, mid-section, and La Paz data, respectively.

Controls on Erosion Patterns

In the Upper Beni River region, channel incision rates appear to control basin-averaged erosion rates. Controls on channel incision rate, in turn, can include climate, tectonic patterns, and lithologic influences. The broad pattern of precipitation in the study area is defined by a maximum in the Sub-Andes and decreasing precipitation with elevation (Hoffman, 1979; Masek *et al.*, 1994). This pattern is negatively correlated with the broad pattern of erosion rates documented in Figure 7a. Hence, precipitation patterns do not appear to control basin-averaged erosion rates regionally.

A weak positive correlation ($R^2 = 0{\cdot}17$, F statistic = 9·5, $p = 0{\cdot}05$) does exist between erosion rate and fraction of basin area above *c*. 3400 m, a proxy for snowline elevation during the last local glacial maximum (LLGM; Klein

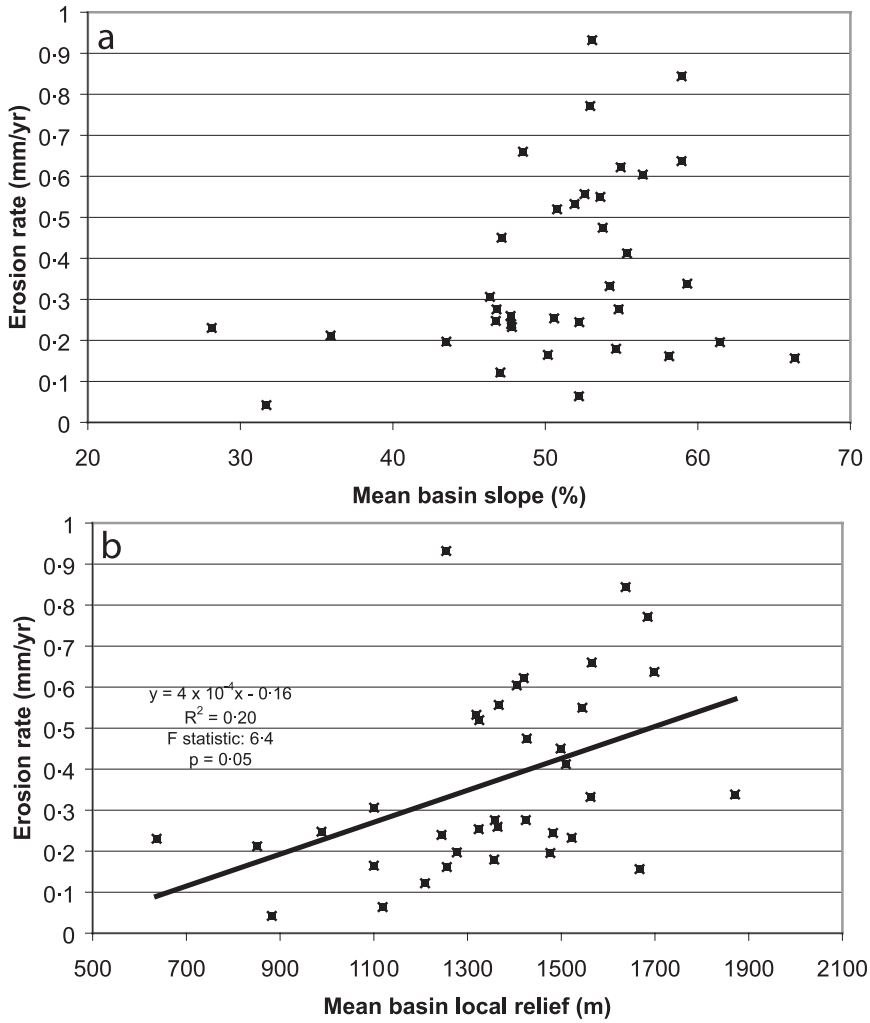

Figure 8. Relationships between basin-averaged erosion rate and morphologic characteristics of hillslopes. (a) Erosion rate versus mean basin slope. (b) Erosion rate versus mean basin local relief.

et al., 1999). However, most of our samples average over timescales shorter than 10^4 years and so were not likely to have been directly affected by altered hydrologic regimes associated with the LLGM. Cosmogenic nuclide production diminishes exponentially with depth over a length scale of *c*. 600 mm. Dividing this distance by a measured erosion rate yields the timescale over which the erosion rate averages. Our erosion rates average over *c*. 400–15 000 years, with 75 per cent of the measurements averaging over *c*. 900–3800 years. Moreover, the two basins that average over time periods ≥10 000 years have no basin area above 3400 m. We observed no obvious indirect effects of glaciation that might elevate subsequent erosion rates, such as significant quantities of stored sediment or widespread landsliding due to valley wall steepening in formerly glaciated portions of the landscape. It may be, therefore, that the correlation between erosion rate and fraction of basin area >3400 m reflects, rather than controls, the relationship between erosion rate and down-basin distance (correlated with elevation) that results from spatial patterns of k_{sn}.

Our data suggest a component of tectonic control on erosion rate patterns. Normalized channel steepness index values increase relatively abruptly near the proposed boundary between the EC and the IAZ (Figure 7), at a down-basin distance of *c*. 80 km, suggesting an uplift rate contrast in this area. Steep channels promote rapid incision which produces high basin-averaged erosion rates, contributing to the observed increase in erosion rate towards the crest of the range. We recognize that there may be many ways to accomplish this uplift contrast kinematically. For example, McQuarrie (2002) argues that the EC and the IAZ are distinguished not only by differences in structural levels and

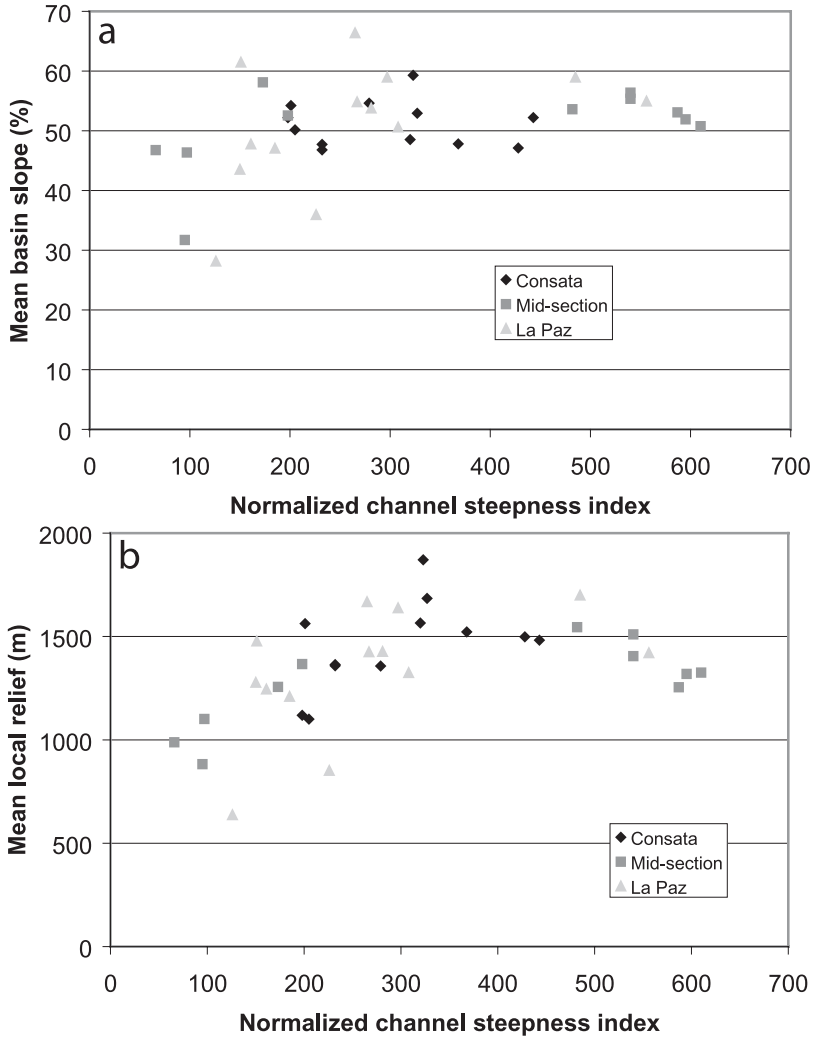

Figure 9. Relationships between morphologic characteristics of hillslopes and normalized channel steepness index. (a) Mean basin slope versus normalized channel steepness index. (b) Mean basin local relief versus normalized channel steepness index. Cross-basin sections are indicated by symbol shade and shape.

timing of deformation but also by underlying basement structures. She argues that the deformed Palaeozoic rocks in the EC are underlain by two Precambrian basement thrust sheets *c*. 10–15 km thick, while the IAZ is underlain only by the younger, and structurally lower, of these. McQuarrie (2002) further posits that this entire rock package is riding over a basement ramp currently located beneath the lower EC, at least in the Cochabamba region, which flattens into a decollement in the IAZ. The fault surface extends into the Sub-Andes, where it climbs through Phanerozoic rocks and localizes active, thin-skinned deformation. This structural scenario implies that the IAZ has already passed over the basement ramp and should therefore have low rates of modern uplift, while the EC should be the locus of relatively rapid uplift. Our data are broadly consistent with this notion but indicate relatively high erosion rates extending all the way to the mountain crest, which demands some mechanism for elevating rock that is not immediately adjacent to the basement ramp. A systematic evaluation of all proposed kinematic models for the Beni region in light of our data is beyond the scope of this paper, but the spatial patterns of erosion that we have defined are relevant to future debates over the tectonic evolution of this range (e.g. Vance *et al*. (2003) for the Himalaya).

Lithology influences erosion rate primarily through rock strength properties. Rock strength and tectonic patterns are related, because strength often reflects the structural depth of rocks brought to the surface in tectonically distinct zones. In the Upper Beni River region, rocks in the EC come from the greatest structural depths and are significantly

stronger on average (t-test with $p = 0{\cdot}05$) than rocks in the Altiplano or IAZ, as indicated by Schmidt hammer measurements. Rock strength patterns may contribute to spatial patterns of normalized channel steepness index, e.g. on the Challana River (Figure 6). However, rock strength does not appear to exert a first-order control on basin-averaged erosion rates. While the occurrence of weak rock may contribute to elevated erosion rates in the upper part of the Consata section, erosion rates in other areas underlain by weak rock (e.g. upper La Paz section, IAZ) are low, and erosion rates in the EC are generally high.

In summary, tectonically induced patterns of channel steepness appear to exert the main control on basin-averaged erosion rates, with lithology playing a secondary role and with no recognizable effect of climate. Our data suggest a possible uplift contrast between the EC and the IAZ. Sub-regional structural histories are currently unavailable, so we cannot determine whether along-strike differences in down-basin erosion patterns stem from local tectonic variations. Alternatively, along-strike differences in erosion pattern may reflect differences in transient channel network incision histories driven by interactions between uplift patterns and channel network topology (Safran, 1998).

Sources of Uncertainty in Erosion Rate Estimates and Implications for Findings

The Upper Beni River basin is a large and complex mountain landscape, and erosion rate estimates derived from it exhibit substantial variability. We have identified broad, systematic patterns in erosion rates and have discussed the factors that appear to drive those patterns. There are also numerous sources of uncertainty stemming from intra-basin processes and from assumptions built into our analytical framework that doubtless contribute to the variability of erosion rates and to the scatter in the relationships we have defined. Here, we discuss some of those sources of uncertainty and their implications for our findings.

In mountainous topography characterized by widespread landsliding, sediment delivery to channels is episodic. This episodicity may introduce temporal variability into erosion rate estimates derived from CRN analysis of alluvium as pulses of more lightly irradiated, landslide-derived sediment move down channel networks. In small basins (tens of km^2), modelling suggests that CRN analysis may systematically underestimate true erosion rates (Niemi *et al*., 2004, in press). Most of our erosion rate estimates are unlikely to be systematically low due to basin size effects, as >90 per cent of our sample basins are >10 km^2 and >60 per cent of them are >70 km^2. Moreover, eliminating basins <70 km^2 from the correlation between basin-averaged erosion rate and normalized channel steepness index produces no significant change in the best-fit linear model or its R^2 value. The consistency we observe in the erosion rate and normalized channel steepness index relationship across a range of basin sizes suggests that our results are not strongly biased by landslide-mediated effects.

In rugged terrain with high local relief, portions of the landscape are partially shielded from radiation. The effects of shielding on CRN-based erosion rate estimates derived from alluvium in mountainous landscapes are complex and have not been documented in this or in previously published studies. Shielding in rugged terrain lowers basin-averaged production rate, both because of 'sky view' and surface slope effects (Dunne *et al*., 1999). At the same time, an increase in neutron attenuation length accompanies a decrease in sky view due to higher average zenith angles for incoming cosmic rays (Dunne *et al*., 1999). Since calculated erosion rate depends on the product of production rate and attenuation length (Lal, 1991), these two shielding effects partially offset one another. However, the decrease in production rate is the stronger effect (Dunne *et al*., 1999). Neglecting shielding may therefore result in an overestimate of basin-averaged erosion rate. The absolute magnitude of this effect in the Upper Beni River basin could be up to several tens of per cent. However, since the entire study area is characterized by rugged topography, we do not expect that shielding substantially affects the relative magnitude of erosion rates among our sample basins and hence the spatial patterns we document.

Characterization of major non-uniformities in quartz distribution is necessary for proper weighting of basin-scale production rates. The richest sources of quartz in the Upper Beni River basin are the granitoid lithologies near the basin headwaters (Figure 2). Etching experiments on six samples from basins partially underlain by granitoids imply relatively low uncertainty about the mapped locations of these rocks because extractable quartz content appears linearly related to the mapped fraction of the basin underlain by granitoids (Figure 10). However, etching experiments also indicate considerable variation in extractable quartz content (<0·5 to 6 per cent) from samples derived from granitoid-free basins. Uncertainty about the details of quartz distribution in non-granitoid lithologies is an additional source of non-systematic variability in our erosion rate estimates.

Uncertainty in k_{sn} values contributes to scatter in the relationship between erosion rate and normalized channel steepness index. We estimate there is *c*. 20 per cent uncertainty on most normalized channel steepness index values, because the DEM from which the values were derived is relatively coarse and because k_{sn} patterns in some basins are complex. Reported values are those that characterize the majority of the mainstem length.

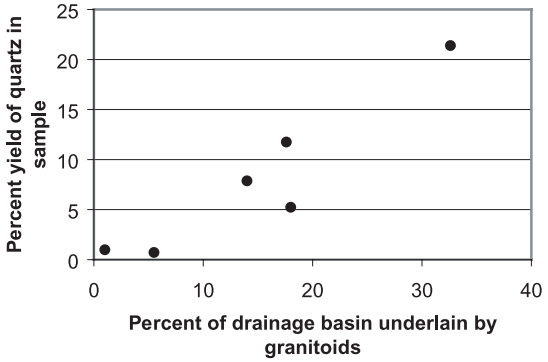

Figure 10. Relationship between percentage yield of quartz and percentage of basin underlain by granitoids. Percentage yield of quartz was determined during acid etching experiments for six samples whose drainage basins are partially underlain by granitoid lithologies, according to geological mapping. Spatial information about outcropping patterns of granitoids was based on a digital version of Figure 2.

Non-uniform erosion within sample basins can potentially bias CRN-derived, basin-averaged erosion rate estimates if there is a systematic relationship between production rate and local erosion rate. For example, if the locus of most rapid erosion within a sample basin is near the valley bottom where production rates are low because of altitudinal and shielding effects, CRN-derived erosion rate estimates may systematically overestimate true erosion rates. If, on the other hand, erosion rates are highest near the elevated basin headwaters for tectonic or climatic reasons, then CRN-based erosion rates may be underestimates. Lack of independent evidence about sub-basin-scale erosion patterns generally precludes incorporation of such complexities into erosion rate estimates. We acknowledge non-uniform erosion as a potential source of uncertainty in our erosion rate estimates but do not have evidence for a systematic bias imposed by that uncertainty.

Conclusions

Mean and modal values of ^{10}Be-derived erosion rates are comparable in magnitude to long-term erosion rates derived from apatite fission track analyses in the Upper Beni River of the Bolivian Andes. Therefore our data imply no dramatic variation in erosion rate during the last several million years.

Erosion rates exhibit a correlation with normalized channel steepness index, which has been elsewhere correlated with incision rate (e.g. Kirby and Whipple, 2001; Lague and Davy, 2003; Wobus *et al*., in press), thus highlighting the influence of channel incision rates on basin-wide erosion patterns. This correlation, combined with spatial patterns of normalized channel steepness index, produces a general down-basin decrease in erosion rate. Basin-averaged erosion rates correlate only weakly or not at all with metrics of hillslope morphology, most likely because many hillslopes are at thresholds of local relief and/or gradient and are morphologically insensitive to variations in erosion rate. Parts of the landscape also appear to be in a transient state of adjustment to channel incision patterns.

Tectonic patterns appear to exert the most significant control over spatial patterns of normalized channel steepness index and, by implication, incision rate, with lithology playing a secondary role. Climate does not appear to exert significant control on patterns of basin-averaged erosion rates. The inferred lack of climatic control on erosion rate is similar to findings of Aalto *et al*. (in press) for the Beni region. The origin of significant differences in normalized channel steepness index patterns among drainages remains ambiguous but may be related to transient channel network incision histories driven by interactions between uplift patterns and channel network topology.

Acknowledgements

This research was supported by a NASA Earth Systems Science Graduate Fellowship and NSF grants EAR-9628737 and EAR-0309688. We thank Ing. Franz Tavera and Eddy Valdellon of SERGEOMIN for logistical support and geologic expertise in the field. We thank Nadine McQuarrie for stimulating discussions of Andean tectonics. We thank Jennifer Larsen, Ben Copans and Megan McGee for the laboratory work essential to this study. We thank Marin Clark and an anonymous reviewer for suggestions that improved this manuscript.

References

Aalto R, Dunne T, Guyot JL. In press. Geomorphic controls on Andean denudation rates. *Journal of Geology*.

Avila-Salinas WA. 1990. Tin-bearing granites from the Cordillera Real, Bolivia; a petrological and geochemical review. In Plutonism from Antarctica to Alaska, Kay SM, Rapela CW (eds). Special Paper 241. Geological Society of America: Boulder, CO; 145–159.

Beaumont C, Fullsack P, Hamilton J. 1992. Erosional control of active compressional orogens. In *Thrust Tectonics*, McClay KR (ed.). Chapman and Hall: London; pp. 1–19.

Benjamin MT, Johnson NM, Naeser CW. 1987. Recent rapid uplift in the Bolivian Andes: Evidence from fission-track dating. *Geology* **15**: 680–683.

Bierman PR, Steig E. 1996. Estimating rates of denudation and sediment transport using cosmogenic isotope abundances in sediment. *Earth Surface Processes and Landforms* **21**: 125–139.

Bierman PR, Caffee M. 2002. Cosmogenic exposure and erosion history of ancient Australian bedrock landforms. *Geological Society of America Bulletin* **114**: 787–803.

Bierman PR, Clapp EM, Nichols KK, Gillespie AR, Caffee M. 2001. Using cosmogenic nuclide measurements in sediments to understand background rates of erosion and sediment transport. In *Landscape Erosion and Evolution Modelling*, Harmon RS, Doe WM (eds). Kluwer: New York; 89–116.

Blodgett TA. 1998. *Erosion rates on the NE escarpment of the Eastern Cordillera, Bolivia, derived from aerial photographs and thematic mapper images*. Cornell University: Ithaca, NY.

Brown ET, Stallard RF, Larsen MC, Raisbeck GM, Yiou F. 1995a. Denudation rates determined from the accumulation of in situ-produced ^{10}Be in the Luquillo Experimental Forest, Puerto Rico. *Earth and Planetary Science Letters* **129**: 193–202.

Brown ET, Bourles DL, Colin F, Raisbeck GM, Yiou F, Desgarceaux S. 1995b. Evidence for muon-induced production of 10Be in near-surface rocks from the Congo. *Geophysical Research Letters* **22**(6): 703–706.

Burbank DW, Leland J, Fielding E, Anderson RS, Brozovic N, Reid MR, Duncan C. 1996. Bedrock incision, rock uplift, and threshold hillslopes in the northwestern Himalayas. *Nature* **379**: 505–510.

Dunne T, Mertes LAK, Meade RH, Richey JE, Forsberg BR. 1998. Exchanges of sediment between the flood plain and the channel of the Amazon River in Brazil. *Geological Society of America Bulletin* **110**: 450–467.

Dunne J, Elmore D, Muzikar P. 1999. Scaling factors for the rates of production of cosmogenic nuclides for geometric shielding and attenuation at depth on sloped surfaces. *Geomorphology* **27**: 3–11.

Flint JJ. 1974. Stream gradient as a function of order, magnitude, and discharge. *Water Resources Research* **5**: 969–973.

Fornari M, Herail G, Viscara G, Laubacher G, Argollo J. 1987. Sedimentation et structure du basin de Tipuani-Mapiri: un temoin de l'evolution du front amazonien des Andes du nord de la Bolivie. *Comptes Rendus de l'Adademie des Sciences, Serie 2* **305**: 1303–1308.

Gabet EJ, Pratt-Sitaula BA, Burbank DW. 2003. Climatic controls on hillslope angle and relief in the Himalayas. *Geology* **32**: 629–632.

Granger DE, Smith AL. 2000. Dating buried sediments using radioactive decay and muonogenic production of ^{26}Al and ^{10}Be. *Nuclear Instruments and Methods in Physics Research B* **172**: 822–826.

Granger DE, Kirchner JW, Finkel R. 1996. Spatially averaged long-term erosion rates measured from in situ-produced cosmogenic nuclides in alluvial sediment. *Journal of Geology* **104**: 249–257.

Guyot JL. 1993. *Hydrogéochimie des fleuves de l'Amazonie Bolivienne*. Études et Thèses. Editions de l'ORSTOM: Paris.

Heisinger B, Lal D, Jull AJT, Kubik P, Ivy-Ochs S, Neumaier S, Knie K, Lazarev V, Nolte E. 2002a. Production of selected cosmogenic radionuclides by muons: 1. Fast muons. *Earth and Planetary Science Letters* **200**: 345–355.

Heisinger B, Lal D, Jull AJT, Kubik P, Ivy-Ochs S, Knie K, Nolte E. 2002b. Production of selected cosmogenic radionuclides by muons: 2. Capture of negative muons. *Earth and Planetary Science Letters* **200**: 357–369.

Herail G, Visarra G. 1988. *El 'cauce antiguo' del Rio Tipuani: Analisis sedimentologico y tectonico e implicaciones para la prospeccion minera*. Convenio UMSA-ORSTOM, Imforme 12.

Hoffman AJ (ed.). 1979. *Climatic Atlas of South America*. World Meteorological Organization, UNESCO: Geneva.

Howard AD, Kerby G. 1983. Channel changes in badlands. *Geological Society of America Bulletin* **94**: 739–752.

Howard AD, Dietrich WE, Seidl, MA. 1994. Modeling fluvial erosion on regional to continental scales. *Journal of Geophysical Research* **99**(B7): 13971–13986.

Kirby E, Whipple K. 2001. Quantifying differential rock-uplift rates via stream profile analysis. *Geology* **29**: 415–418.

Kirby E, Whipple K, Tang W, Chen Z. 2003. Distribution of active rock uplift along the eastern margin of the Tibetan Plateau: inferences from bedrock channel longitudinal profiles. *Journal of Geophysical Research* **108**. DOI:10.1029/2001JB000861.

Kirchner JW, Finkel RC, Riebe CS, Granger DE, Clayton JL, King JG, Megahan WF. 2001. Mountain erosion over 10 yr, 10 k.y., and 10 m.y. time scales. *Geology* **29**: 591–594.

Klein AG, Seltzer, GO, Isacks BL. 1999. Modern and last local glacial maximum snowlines in the Central Andes of Peru, Bolivia, and Northern Chile. *Quaternary Science Reviews* **18**: 63–84.

Kohl CP, Nishiizumi K. 1992. Chemical isolation of quartz for measurement of *in-situ* – produced cosmogenic nuclides. *Geochimica et Cosmochimica Acta* **56**: 3583–3587.

Lague D, Davy P. 2003. Constraints on the long-term colluvial erosion law by analyzing slope-area relationships at various tectonic uplift rates in the Siwaliks Hills (Nepal). *Journal of Geophysical Research, B, Solid Earth and Planets* **108**. DOI:10.1029/2002JB001893.

Lal D. 1991. Cosmic ray labeling of erosion surfaces; in situ nuclide production rates and erosion models. *Earth and Planetary Science Letters* **104**: 424–439.

Lavé J, Avouac JP. 2000. Active folding of fluvial terraces across the Siwaliks Hills, Himalayas of central Nepal. *Journal of Geophysical Research* **105**: 5735–5770.

Lavé J, Avouac JP. 2001. Fluvial incision and tectonic uplift across the Himalayas of central Nepal. *Journal of Geophysical Research* **106**: 26561–26591.

Martinez C. 1980. *Structure et évolution de la châine hercynienne et de la châine andine dans le nord de la Cordillère des Andes de Bolivie*. Travaux e Documents 119. l'ORSTOM: Paris.

Martinez C, Tomasi P. 1978. *Carte structurale des Andes septentrionales de Bolivie – Mapa estructural de los Andes septentrionales de Bolivia*. ORSTOM: Paris.

Masek JG, Isacks BL, Gubbels TL, Fielding EJ. 1994. Erosion and tectonics at the margins of continental plateaus. *Journal of Geophysical Research* **99**: 13 941–13 956.

Matmon A, Bierman PR, Larsen J, Southworth S, Pavich M, Caffee M. 2003. Temporally and spatially uniform rates of erosion in the southern Appalachian Great Smoky Mountains. *Geology* **31**: 155–158.

McQuarrie N. 2002. The kinematic history of the central Andean fold-thrust belt, Bolivia: Implications for building a high plateau. *Geological Society of America Bulletin* **114**: 950–963.

Montgomery DR, Foufoula-Georgiou E. 1993. Channel network representation using digital elevation models. *Water Resources Research* **29**: 1178–1191.

Montgomery DR, Brandon MT. 2002. Topographic controls on erosion rates in tectonically active mountain ranges. *Earth and Planetary Science Letters* **201**: 481–489.

Niemi N, Oskin M, Burbank D. 2004. A numerical simulation of the effects of mass-wasting on cosmogenically determined erosion rates. *Eos Transactions AGU 85: Fall Meeting Supplement*: Abstract H51C-1157.

Niemi N, Oskin M, Burbank D, Heimsath A. In press. A numerical simulation of the effects of bedrock landsliding on cosmogenically determined erosion rates. *Earth and Planetary Science Letters*.

Nishiizumi K, Winterer EL, Kohl CP, Klein J, Middleton R, Lal D, Arnold JR. 1989. Cosmic ray production rates of ^{10}Be and ^{26}Al in quartz from glacially polished rocks. *Journal of Geophysical Research, B, Solid Earth and Planets* **94**: 17907–17915.

Reiners PW, Ehlers TA, Mitchell SG, Montgomery DR. 2003. Coupled spatial variations in precipitation and long-term erosion rates across the Washington Cascades. *Nature* **426**: 645–647.

Roering JJ, Kirchner KW, Dietrich WE. 2001. Hillslope evolution by nonlinear, slope-dependent transport; steady state morphology and equilibrium adjustment timescales. *Journal of Geophysical Research, B, Solid Earth and Planets* **106**: 16499–16513.

Safran EB. 1998. *Channel network incision and patterns of mountain geomorphology*. University of California, Santa Barbara: Santa Barbara, CA.

Schaller M, von Blanckenburg F, Hovius N, Kubik PW. 2001. Large-scale erosion rates from in situ-produced cosmogenic nuclides in European river sediments. *Earth and Planetary Science Letters* **188**: 441–458.

Schmidt KM, Montgomery DR. 1995. Limits to relief. *Science* **270**: 617–620.

Seidl MA, Dietrich WE. 1992. The problem of channel erosion into bedrock. *Catena Supplement* **23**: 101–124.

Sklar L, Dietrich WE. 1998. River longitudinal profiles and bedrock incision models: Stream power and the influence of sediment supply. In *Rivers over Rock, Fluvial Processes in Bedrock Channels*, Tinkler KE, Wohl EE (eds). Geophysical Monograph 107. American Geophysical Union: Washington, DC; 237–260.

Snyder NP, Whipple KX, Tucker GE, Merritts DJ. 2000. Landscape response to channel forcing: DEM analysis of stream profiles in the Mendocino triple junction region, northern California. *Geological Society of America Bulletin* **112**: 1250–1263.

Stephenson R, Lambeck K. 1985. Erosion-isostatic rebound models for uplift; an application to south-eastern Australia. *Geophysical Journal of the Royal Astronomical Society* **82**: 31–55.

Strahler AN. 1950. Equilibrium theory of erosional slopes approached by frequency distribution analysis; Part 1. *American Journal of Science* **248**: 673–696.

Stock J, Dietrich WE. 2003. Valley incision by debris flows; evidence of a topographic signature. *Water Resources Research* **39**. DOI: 10.1029/2001WR001057.

Tarboton DG, Bras RL, Rodriguez-Iturbe I. 1989. Scaling and elevation in river networks. *Water Resources Researc*h **25**: 2037–2051.

Trimble SW. 1977. The fallacy of stream equilibrium in contemporary denudation studies. *American Journal of Science* **277**: 876–887.

Vance D, Bickle M, Ivy-Ochs S, Kubik PW. 2003. Erosion and exhumation in the Himalaya from cosmogenic isotope inventories of river sediments. *Earth and Planetary Science Letters* **206**: 273–288.

Whipple KX. 2004. Bedrock rivers and the geomorphology of active orogens. *Annual Review of Earth and Planetary Sciences* **32**: 151–185.

Wobus CW, Hodges KV, Whipple KX. 2003. Has focused denudation sustained active thrusting at the Himalayan topographic front? *Geology* **31**: 861–864.

Wobus C, Whipple K, Kirby E, Snyder N, Johnson J, Spyropolou K, Crosby B, Sheehan D. In press. Tectonics from topography: Procedures, promise, and pitfalls. In *Climate, Tectonics, and Landscape Evolution*, Willett S, Hovius N, Brandon M, Fisher D (eds). Geological Society of America Special Paper.

